Journal of Molecular Catalysis A: Chemical 315 (2010) 51–59

Contents lists available at ScienceDirect

Journal of Molecular Catalysis A: Chemical

journal homepage: www.elsevier.com/locate/molcata

Immobilization of chiral cationic diphosphine rhodium complexes in nanopores of mesoporous silica and application in asymmetric hydrogenation

Reine Sayah [a,b], Marie Le Floch [c], Eric Framery [b,*], Véronique Dufaud [a,**]

[a] Laboratoire de Chimie, UMR 5182 ENS/CNRS, Ecole Normale Supérieure de Lyon, 46 allée d'Italie, F-69364 Lyon Cedex 07, France
[b] ICBMS, UMR-CNRS 5246, Equipe Synthèse Asymétrique, Université de Lyon, Université Lyon 1, 43 boulevard du 11 Novembre 1918, F-69622 Villeurbanne Cedex, France
[c] UMR-CNRS 6226 Sciences Chimiques de Rennes, Equipe "Verres et Céramiques", Campus de Beaulieu, Université de Rennes 1, 35042 Rennes-Cedex, France

ARTICLE INFO

Article history:
Received 30 March 2009
Received in revised form 30 August 2009
Accepted 31 August 2009
Available online 6 September 2009

Keywords:
Asymmetric hydrogenation
Chiral cationic rhodium complex
DIOP ligand
Mesoporous hybrid material
Covalent immobilization

ABSTRACT

Heterogeneous chiral cationic rhodium complexes bearing bidentate phosphine derived from (−)-2,2-dimethyl-4,5-bis(diphenylphosphino)methyl)-1,3-dioxolane (DIOP) were prepared by covalent immobilization onto SBA type silica. In order to introduce the tether to the surface, it was necessary to modify chemically the DIOP ligand through a reaction sequence consisting of hydrolysis and condensation with organosiloxane precursor. Two types of cationic rhodium hybrid materials based on SBA-15 and partially capped SBA-3 type silica were prepared under classical grafting procedures. The catalytic solids were fully characterized using a wide variety of molecular and solid-state techniques to determine their structural and textural properties. The performances of these latter were then evaluated in the hydrogenation of methyl (*Z*)-2-*N*-acetylaminocinnamate under various reaction conditions (pressure and temperature). Generally, the activity of supported catalysts was high as full conversions were obtained but immobilization of the system leads to significant loss of enantioselectivity. The best ee (20%) was observed in the case of the catalyst whose surface had been passivated prior to the grafting but the enantiomeric excesses were fairly below the values of the homogeneous catalysis.

© 2009 Elsevier B.V. All rights reserved.

1. Introduction

The synthesis of environmentally friendly catalysts which respond to the criteria of green chemistry is an on-going challenge in asymmetric catalysis. Current studies focus on the development of more efficient methods for precious metal (toxic in many cases) and expensive ligand recovery and reuse, as well as the reduction of costs and waste. In this respect, heterogeneous catalysts immobilized on insoluble inorganic [1] or organic [2] supports represent attractive alternatives to the homogeneous systems. On the other hand, high activity and better control of stereoselectivity are generally easier to achieve with homogeneous systems, as heterogeneous systems are often reported as less reactive and less predictable in terms of selectivity and enantioselectivity [[3] and references cited therein]. To address this problem, that is, maintain efficient recovery and recycling while keeping the high selectivity of solution catalysts, various methods have been developed for the anchoring of transition metal complexes onto organic or inorganic solid carriers including entrapment, adsorption, ion-pair formation and covalent binding [4].

The researcher who adopts the latter strategy, covalent anchoring, is undertaking a risky endeavour as the modification of ligands needed to add the covalent link to the surface can be challenging and time-consuming, and furthermore the modified ligand can differ from the unmodified model in important and unpredictable ways. When this approach succeeds, it can pay off with significant benefits; among those is the greater stability of the immobilized species when covalent links are used in the immobilization process, leading to reduction of leaching and thus metal contamination of the products.

Chiral C_2-symmetric diphosphines, such as DIOP [5], DIPAMP [6], Chiraphos [7], DuPhos [8] and BINAP [9], and their corresponding rhodium complexes are of special interest due to their effectiveness in many homogeneous asymmetric hydrogenation reactions. Over the past decade numerous studies have been devoted to their immobilization using different strategies. One approach involves the noncovalent anchoring of chiral diphosphine metal complexes onto silica or modified silica matrix. Augustine et al. [10] have recently reported an efficient method for the heterogenization of ionic transition metal complexes *via* an ionic interaction between positive charge of the metal and the negative charge of the silica surface employing heteropoly acids as the anchor. Following this approach, various cationic chiral rhodium complexes derived

* Corresponding author. Tel.: +33 4 72 44 62 63; fax: +33 4 72 44 81 60.
** Corresponding author. Tel.: +33 4 72 72 88 57; fax: +33 4 72 72 88 60.
E-mail addresses: Eric.Framery@univ-lyon1.fr (E. Framery), Veronique.Dufaud@ens-lyon.fr (V. Dufaud).

1381-1169/$ – see front matter © 2009 Elsevier B.V. All rights reserved.
doi:10.1016/j.molcata.2009.08.025

from *S*,*S*-/*R*,*R*-Me-Duphos, *R*,*R*-DIOP, (+)-Norphos, *S*,*S*-Chiraphos and *S*,*S*-DIPAMP, have been immobilized by electrostatic binding onto the surface of MCM-41 [11], Al-MCM-41 [12], Al-SBA-15 [12b] or AlTUD-1 [13] yielding relatively stable and effective catalysts although generally less enantioselective than their soluble analogues. The nature of the support is also of crucial importance in achieving high enantioselectivity and robustness towards leaching. For example, the aluminum sites in Al-MCM-41 play an important role in the interaction with the cationic rhodium center. In the immobilization of Rh-complexes derived from *R*,*R*-Me-Duphos and *R*,*S*-Josiphos, Hems et al. [12b] have compared the influence of two types of silica supports, Al-MCM-41 and Al-SBA-15. Although these hybrid materials were efficient catalysts in the hydrogenation of dimethylitaconate or methyl-2-acetamidoacrylate with performances comparable to those observed for the homogeneous complex, their stability toward leaching varied significantly. When MCM-41 was used as the support, the catalyst could be readily reused without loss of catalytic performance whereas in the case of SBA-15 type silica, alteration of the rate and enantioselectivity was observed during catalyst recycling. This instability was ascribed to the basic structure of Al-SBA-15 in which the Al centers embedded within the pore walls would be less accessible to the cationic rhodium than in Al-MCM-41. The choice of solvent is also extremely important, influencing the activity, and also the enantioselectivity and the stability of the immobilized metal species as demonstrated by Simons et al. when mesoporous aluminosilicate AlTUD-1 network was used [13].

To our knowledge, few examples of chiral diphosphine metal complexes anchored to mesoporous silica support via covalent bonding have been reported. One of the first examples is the work of Raynor et al. [14] which involved the covalent grafting of chiral Pd-catalyst derived from 1,1′-bis(diphenylphosphino)ferrocene onto MCM-41. This confined catalyst displayed enhanced enantioselectivity and activity in the hydrogenation of ethyl nicotinate to ethyl nipecotinate compared to its analogous homogeneous model. In a 2001 report, an achiral bidentate rhodium phosphine complex was grafted onto the surface of SBA-15 type silica in the presence and in the absence of an unfunctionalized ethyltrialkoxysilane, $EtSi(OEt)_3$, used as a spacer in order to prevent the formation of P(V) species [15]. The heterogeneous Rh-catalyst prepared at room temperature in the presence of $EtSi(OEt)_3$ exhibited the highest activity in hydrogenation of isosafrole (TON of 3300), probably due to site isolation of the catalyst on the surface [16]. Chiral bisphosphine-based ligands such as MeO-Biphep and Biphemp anchored to commercially silica gel (Grace 332) [17] showed good enantiomeric excesses and TONs but relatively low rates when associated with ruthenium for the hydrogenation of methyl phenylglyoxylate. The rhodium catalysts were less effective for the hydrogenation of methyl (*Z*)-2-*N*-acetylaminocinnamate, enantioselectivies not exceeding 45% but with rather high rates.

In the present contribution, we report on the chemical modification of (−)-2,2-dimethyl-4,5-bis(diphenylphosphino)methyl)-1,3-dioxolane (DIOP) in order to prepare new cationic Rh-complexes which were anchored using covalent bonds to the surface of SBA-15 and partially capped SBA-3 type silica. The state of the solid structure and the integrity of the molecular complexes were characterized by several methods including X-ray powder diffraction at small angles, elemental analysis, thermogravimetric analysis, infrared spectroscopy, multi-nuclei solid-state NMR spectroscopy and nitrogen sorptions. These new supported catalysts have been evaluated in the hydrogenation of methyl (*Z*)-2-*N*-acetylaminocinnamate. The DIOP ligand was chosen for its *modest* enantiodiscrimination for this asymmetric hydrogenation, generally around 60% [5,18] which would allow the observation of subtle effects of the heterogenization has on performance.

2. Experimental

2.1. General

All manipulations were conducted under a strict inert atmosphere or vacuum conditions using Schlenk techniques including the transfer of the catalysts to the reaction vessel. The solvents were dried using standard methods and stored over activated 4A molecular sieves. Tetraethoxysilane (TEOS), poly(ethyleneoxide)–poly(propyleneoxide)–poly(ethyleneoxide) block copolymer (Pluronic 123, Mw 5000) were purchased from Aldrich Chemical and used without further purification. Cetyltrimethylammonium bromide (CTAB) and (−)-2,2-dimethyl-4,5-bis[(diphenylphosphino)methyl]-1,3-dioxolane (DIOP) were obtained from Acros. (3-Isocyanatopropyl)triethoxysilane was purchased from ABCR and chloro-(1,5-cyclooctadiene)rhodium (I) dimer from Alfa Aesar.

The disphosphine diop-diol, (−)-1,4-bis(diphenylphosphino)butane-2,3-diol, was cleanly obtained through hydrolysis of diop with perchloric acid at room temperature [19]. The cationic $[Rh(COD)_2]^+BF_4^-$ was prepared by reacting $[Rh(COD)C1]_2$ with $AgBF_4$ in the presence of 1,5-cyclooctadiene according to procedures previously described in the literature [20]. The starting compound to be hydrogenated, methyl (*Z*)-2-*N*-acetylaminocinnamate, was synthesized as described elsewhere [21].

2.2. Silylation of diop-diol diphosphine [17]

2.2.1. Synthesis of (2S,3S)-1,4-bis(diphenylphosphino)butane-2,3-diyl-bis[(3-triethoxysilyl)propyl)carbamate] **1**

(−)-1,4-Bis(diphenylphosphino)butane-2,3-diol (0.30 g, 0.65 mmol) was dissolved in dry THF (9 mL) followed by dropwise addition of (3-isocyanatopropyl)triethoxysilane (0.48 g, 1.96 mmol) and $Bu_2Sn(laurate)_2$ as the catalyst. The resulting mixture was stirred at 65 °C for 24 h. The solvent was then removed under reduced pressure and the residue extracted with hexane (3× 15 mL) yielding **1** as a mixture of bis-silylated (**1a**, 23%) and mono-silylated (**1b**, 77%) product.

Eluent ethyl acetate/pentane = 30/70. R_f = 0.7. 96% as a colourless oil. ^{1}H NMR (200 MHz, $CDCl_3$): δ ppm: 7.72–7.28 (m, 20H, H_{Ar}), 5.12 (brs, 2H, NH), 4.59 (t, 2H, ^3J = 5.4 Hz, CH), 3.70 (q, 12H, ^3J = 7.0 Hz, OCH_2), 3.12–3.03 (m, 4H, CH_2NH), 2.49–2.22 (m, 4H, CH_2PPh_2), 1.61–1.46 (m, 4H, CH_2CH_2NH), 1.2 (t, 18H, ^3J = 7 Hz, OCH_2CH_3), 0.57 (t, ^3J = 8.2 Hz, CH_2Si). ^{13}C NMR (50 MHz, $CDCl_3$): δ ppm: 155.6 (C=O), 138.7 (C_{ipso}, d, $^1J_{(C-P)}$ = 13.2 Hz, C_{Ar}), 138.1 (C_{ipso}, d, $^1J_{(C-P)}$ = 13.0 Hz, C_{Ar}), 133.1 (C_{ortho}, d, $^2J_{(C-P)}$ = 19.4 Hz, C_{Ar}), 128.7–128.5 (C_{Ar}), 72.7 (d, $^2J_{(C-P)}$ = 14.3 Hz, $CHCH_2P$), 72.6 (d, $^2J_{(C-P)}$ = 8.2 Hz, $CHCH_2P$), 58.5 (CH_3CH_2O), 43.1 (CH_2NH of propyl chain), 31.1 (d, $^1J_{(C-P)}$ = 13.2 Hz, $CHCH_2P$), 23.7 ($SiCH_2CH_2CH_2$ of propyl chain), 18.4 (CH_3CH_2O), 7.7 ($SiCH_2CH_2CH_2$ of propyl chain). ^{31}P NMR (81 MHz, $CDCl_3$): δ ppm: −23.2. $[\alpha]_D^{20} = -5.2$ (CH_2Cl_2, C = 1.0).

2.3. Catalyst preparation

2.3.1. Homogeneous catalysts

2.3.1.1. Synthesis of {(2S,3S)-1,4-bis(diphenylphosphino)butane-2,3-diyl-bis[((3-triethoxysilyl)propyl)carbamate]} (1,5-cyclooctadiene) tetrafluoroborate of rhodium (I) 2.

1 (0.30 g, 0.31 mmol) dissolved in degassed toluene (10 mL) was added dropwise to a solution of $Rh(COD)_2^+BF_4^-$ (0.12 g, 0.31 mmol) in degassed toluene (10 mL). The reaction mixture was stirred at room temperature for 3 h. **2** was quantitatively obtained after solvent removal as a mixture of **2a** (bis-silylated diop) and **2b** (mono-silylated diop).

Yield: 100% as a light orange solid. ^{13}C NMR (50 MHz, $CDCl_3$) δ ppm: 155.2 (C=O), 131.8–128.6 (C_{Ar}), 58.4 (CH_3CH_2O), 53.4 (CH_2NH of propyl chain), 43.2 (d, $^2J_{(C-P)}$ = 31 Hz, $CHCH_2P$), 28.0 ($SiCH_2CH_2CH_2$ of propyl chain and COD), 23.3 ((d, $^1J_{(C-P)}$ = 25.0 Hz, $CHCH_2P$), 18.3 (CH_3CH_2O), 7.6 ($SiCH_2CH_2CH_2$ of propyl chain).

For **2** (as a mixture of **2a** and **2b**): ^{31}P NMR (81 MHz, toluene-d8) δ ppm: 20.9 (dd, 1P, $^2J_{P-P}$ = 36.6 Hz and $^1J_{P-Rh}$ = 136.6 Hz, PPh_2 of **2b**), δ 20.9 (d, 0.3P, $^1J_{P-Rh}$ = 136.6 Hz, PPh_2 of **2a**), δ 14.9 (d, 0.3P, $^1J_{P-Rh}$ = 145.4 Hz, PPh_2 of **2a**), 5.6 (dd, 1P, $^2J_{P-P}$ = 36.6 Hz and $^1J_{P-Rh}$ = 136.6 Hz, PPh_2 of **2b**).

For **2a**: ^{31}P NMR (81 MHz, $CDCl_3$) δ ppm: 25.5 (d, 1P, $^1J_{(P-Rh)}$ = 148.6 Hz, PPh_2); 17.0 (d, 1P, $^1J_{(P-Rh)}$ = 146.4 Hz, PPh_2). MS ($C_{36}H_{52}N_2O_{10}P_2RhSi_2BF_4$) $[M+Na]^+$: found: 1163.10 (calculated: 1163.40).

2.3.2. Heterogeneous catalysts

*2.3.2.1. General procedure for the covalent immobilization of **2** on SBA-15 silica.* SBA-15 type silica was prepared by the acid catalyzed, non-ionic assembly pathway described elsewhere [22]. The structure-directing agent (Pluronic 123) was removed by calcination in air at 500 °C, and the organic-free mesoporous silica was rigorously dried under a flow of nitrogen at 200 °C prior to the grafting reaction.

2 (0.30 g, 0.24 mmol) dissolved in dry toluene was added dropwise to a suspension of calcined SBA-15 (1 g) in toluene and stirred at 25 °C overnight to allow the diffusion of the molecular precursor into the channels of the pores. The reaction mixture was then heated to 65 °C for 15 h. After filtration, the unreacted rhodium precursor was removed by thoroughly washing the solid with toluene and CH_2Cl_2. Finally, the resulting solid was dried in vacuo at 30 °C. The organometallic-inorganic hybrid material, denoted by **[2]/SBA-15**, has been characterized by several analytical, physical and spectroscopic techniques including small-angle X-ray powder diffraction, nitrogen sorption isotherms, and solid-state ^{31}P and ^{29}Si NMR spectra as well as TGA and elemental analyses.

ICP-AES analysis for **[2]/SBA-15** (yellow solid): 1.5 wt% Rh, 1.0 wt% P, and 0.16 wt% B.

*2.3.2.2. General procedure for the covalent immobilization of **2** on SBA-3 type silica.* Partially capped SBA-3 type silica was first prepared according to the procedure described by Dufaud et al. [23] using the following molar composition: TEOS, 1; H_2O, 120; CH_3CN, 4.3; HCl, 9.2; CTAB, 0.12. In a typical procedure, CTAB (4.64 g, 12.80 mmol) was first dissolved in water (118 g), HCl 37% (58 mL, 0.68 mol) and half of the amount of acetonitrile (13.22 g, 0.32 mol) followed by addition of TEOS (15.40 g, 74.00 mmol) solubilized in the remaining portion of acetonitrile. This gel was stirred for 3 h at room temperature. The solid product was recovered by filtration, washed with water and dried under vacuum overnight at 25 °C. The post-silylation reaction was performed in dry toluene (100 mL) at 50 °C for 1 h using $(CH_3)_3SiCl$ (3 mL/1 g of as-made material) as silylating agent. Finally, the template was removed from the as-made material by batch extraction with dry ethanol (40 mL) at 50 °C for 2 h. Three extraction cycles were necessary to complete the process leading to a partially capped SBA-3 silica material.

2 (0.70 g, 0.55 mmol) dissolved in a mixture of toluene/CH_2Cl_2 (30 mL) was then slowly added to a suspension of SBA-3 (0.70 g) in anhydrous and degassed toluene and the reaction mixture was heated at 65 °C. The subsequent steps are similar to those described for the grafting of **2** on SBA-15. The resulting solid is referred to as **[2]/SBA-3**.

Analyze ICP-AES for **[2]/SBA-3**: 2.74 wt% Rh, 1.53 wt% P, and 0.30 wt% B.

2.4. Characterization

Low-angle X-ray powder diffraction (XRD) data were acquired on a Bruker D5005 diffractometer using Cu Kα monochromatic radiation (λ = 1.054184 Å). Nitrogen adsorption–desorption isotherms at 77 K were measured using a Micromeritics ASAP 2010M physisorption analyzer. The samples were evacuated at 160 °C for 24 h before the measurements. Specific surface areas were calculated following the BET procedure. Pore size distribution was obtained by using the BJH pore analysis applied to the desorption branch of the nitrogen adsorption/desorption isotherm. Infrared spectra were recorded from KBr pellets using a Mattson 3000 IRFT spectrometer. A Netzsch thermoanalyser STA 409PC was used for simultaneous thermal analysis combining thermogravimetric analysis (TGA) and differential thermoanalysis (DTA) at a heating rate of 10 °C min^{-1} in air from 25 to 1000 °C. Solid-state NMR spectra were recorded on a Bruker Avance-300 spectrometer using 4 mm diameter ZrO_2 rotors. ^{13}C NMR spectra (75.49 MHz) were obtained with a standard 1D CP-MAS ^{13}C–^{1}H sequence with a spin rate of 12,000 Hz to remove the chemical shift anisotropy and thus the side bands from the 0 to 200 ppm region (contact time: 2 ms, recycle time: 10 s). For the ^{31}P NMR spectra (121.53 MHz) a pulse length of 2 μs with a recycle time of 20 s was used. The chemical shifts are given relative to external 85% H_3PO_4. The ^{29}Si MAS spectra (59.64 MHz) were recorded by using a pulse length of 3 μs, a contact time of 3.5 ms and a recycle time of 10 s. The spinning rate was 10,000 Hz and the chemical shifts are given relative to TMS. CP-MAS ^{29}Si solid NMR measurements were collected on a Bruker DSXv400 spectrometer at a frequency operating at 79.49 MHz. A 5 ms ($y = p/2$) pulse was used with a repetition time of 80 s.

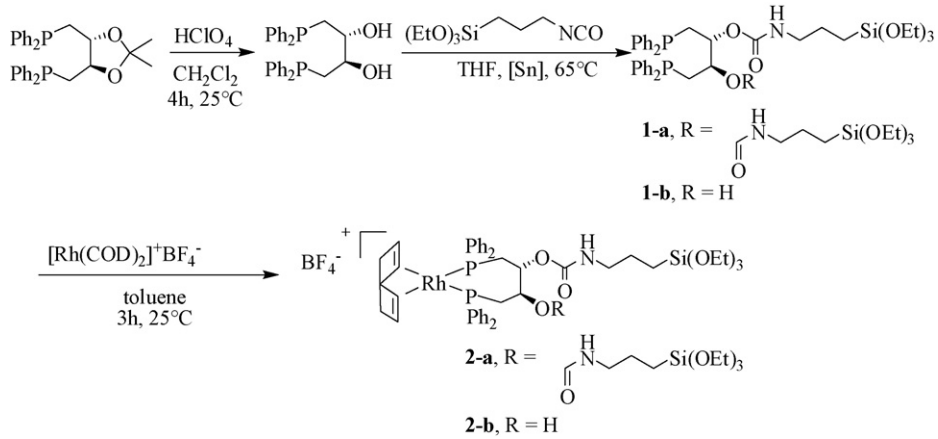

Scheme 1. Silylation of DIOP and generation of rhodium complex **2**.

Liquid NMR spectra were recorded on a Bruker AC-300 spectrometer and referenced as following: ^{1}H (300 MHz), internal $SiMe_4$ at $\delta = 0.00$ ppm, ^{13}C (75 MHz), internal $CDCl_3$ at $\delta = 77.2$ ppm, and ^{31}P (121 MHz), external 85% H_3PO_4 at $\delta = 0.00$ ppm. Mass spectral analyses were performed on a Nermag R10-10C for exact mass. Metal determinations were performed by ICP-OES (Activa Jobin Yvon) spectroscopy from a solution obtained by treatment of the solid catalyst with a mixture of HF, HNO_3 and H_2SO_4 in a Teflon reactor at 150 °C. Flash chromatography was performed under nitrogen at a pressure slightly greater than atmospheric pressure using silica (Merck Silica Gel 60, 230–400 mesh). Thin layer chromatography was performed on Merck Silica Gel 60 F_{254}.

GC analyses were performed on a Varian CP-3800 gas chromatograph equipped with a flame ionization detector, a Varian CP-8400 autosampler and a CP-Sil5CB capillary column (30 m, 0.32 mm internal diameter, 0.25 μm film thickness). Nitrogen was used as carrier gas. Optical rotations were recorded using a PerkinElmer 241 polarimeter. Enantiomeric excess was determined by HPLC with a Chiralpak^{AD} column (25 cm × 4.6 mm) using a 90/10 ratio of hexane/isopropyl alcohol as eluent.

2.5. Catalytic test

The catalytic reactions were carried out in a high pressure stainless steel autoclave (Parr-Equilabo, 300 mL) fitted with a glass liner, temperature regulator and a valve to allow sampling the reaction mixture while the reaction is in process. Conversion and yield were determined by GC based on relative area of the GC-signals referred to an internal standard (diethylene glycol di-*n*-butyl ether) calibrated to the corresponding pure compounds.

2.5.1. General procedure for hydrogenation reactions

In a first Schlenk, 1.14×10^{-2} mmol of $[Rh(COD)]_2{}^{+}BF_4{}^{-}$ were reacted with 2.24×10^{-2} mmol of phosphine in 5 mL of isopropyl alcohol (previously deaerated) for 30 min. In the mean time, a solution composed of 0.25 g (1.14 mmol) of (*Z*)-methyl-2-acetamido-3-phenylacrylate, 0.05 g (0.24 mmol) of diethylene glycol di-*n*-butyl ether (internal standard) and 18 mL of degassed isopropyl alcohol was prepared and transferred onto the catalytic solution. The autoclave, containing a magnetic stirring bar, was then charged with the reaction mixture under a nitrogen atmosphere. The autoclave was sealed, flushed first with nitrogen (7 bar) then with hydrogen (10 bar) by repeated pressurization and release and then pressurized with the desired hydrogen pressure. The temperature was then adjusted to the desired value.

The reaction was monitored by GC until completion of the reaction. At the end of the reaction, the autoclave was opened and the solution filtered through a celite pad. After removal of the solvent under reduced pressure, the reaction products were analyzed by HPLC on a chiral column to determine the enantiomeric excess.

A similar procedure was followed for heterogeneous hydrogenation reactions except that the hybrid catalyst (1.14×10^{-3} mmol of Rh based on elemental analysis) was first evacuated at 40 °C for 4 h to remove physisorbed water.

3. Results and discussion

3.1. Synthesis of molecular rhodium precursor

The first step to prepare covalently bound chiral rhodium catalyst requires ligand structural modification to introduce polycondensable organosiloxane precursor moieties (Scheme 1). This was achieved in two steps. Hydrolysis of diop ligand with perchloric acid at room temperature gave rise to the disphosphine diop-diol, (−)-1,4-bis(diphenylphosphino)butane-2,3-diol, in 76% yield [19]. The reaction of the free hydroxyl groups with (3-isocyanatopropyl)triethoxysilane in the presence of $Bu_2Sn(laurate)_2$ as the catalyst [17] led to the formation of **1** as a mixture of bis-silylated (**1a**, 23%) and mono-silylated (**1b**, 77%) product as determined by ^{1}H NMR. The ^{31}P NMR spectrum of **1** is characterized by the presence of a single resonance at −23.2 ppm typical of free phosphine ligand. The rhodium complex **2** was prepared quantitatively by mixing **1** with 1 equiv. of $Rh(COD)_2{}^{+}BF_4{}^{-}$ in toluene. Upon complexation, the ^{31}P NMR spectrum of **2** exhibited three sets of resonances of different multiplicity (Supporting Information, Fig. S1). The two doublets of doublets at δ 20.9 and δ 5.6 ($^{2}J_{P-P} = 36.6$ Hz and $^{1}J_{P-Rh} = 136.6$ Hz) were attributed to the phosphorus atoms of complex **2b**. The appearance of two distinct signals was expected since the two phosphorous centers are no longer equivalent in this complex. We also observed a doublet at δ 14.9 ($^{1}J_{P-Rh} = 145.4$ Hz) which would correspond to one of the phosphorous atoms of complex **2a**. The resonance corresponding to the second phosphorous atom of **2a** appears to be masked by the more intense peak of complex **2b** at δ 20.9, as evidenced by the integrals and given the chemical shift observed for pure **2a** (Supporting Information, Fig. S2).

3.2. Synthesis of hybrid materials

Two types of periodic mesoporous silica differing in their physical and textural properties as well as by their hydrophobic/hydrophilic properties were used in this study: unmodified SBA-15 type silica and SBA-3 type silica whose surface had been previously organically modified.

SBA-15 type silica is well-suited as a support for immobilizing functional groups. Its large, uniform pore diameter (∼6 nm) provides ample room for reactant and product diffusion, and its thick walls provide hydrothermal stability. The covalent grafting of **2** onto organic-free SBA-15 silica was performed in toluene at relatively low temperature to maintain the integrity of the precursor (65 °C, 15 h). The unreacted rhodium complex was removed by thoroughly washing the solid with toluene and methylene chloride leading to hybrid material **[2]/SBA-15** (Scheme 2).

Mesostructured SBA-3 type silica whose surface had been previously organically modified was used to increase the functional homogeneity of the surface and to prevent undesirable interactions between the metal centre and the surface silanols during the grafting procedure. The synthesis of partially capped silica was achieved in three steps according to a procedure reported by one of the authors [23] and is illustrated in Scheme 3. Typically, the condensation of tetraethylorthosilicate (TEOS) was carried out in the presence of CTAB as structure-directing agent (SDA) under mild, acidic conditions using a binary acetonitrile/water solvent system. The mesostructure of the material was then stabilized by introduction of a silylation step with $(CH_3)_3SiCl$ before SDA removal. This sequential stepwise approach provides a well defined functionalized silica surface in which the trimethylsilyl functions are homogeneously distributed within the pores of the material. Note that during the trimethylsilylation procedure most of the surfac-

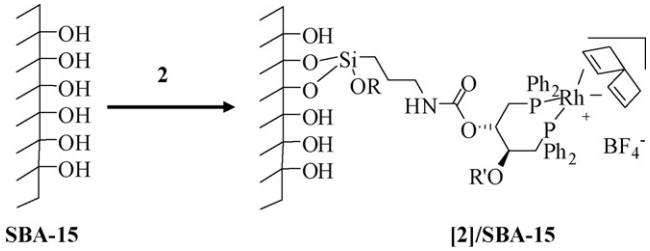

Scheme 2. Grafting of rhodium complex **2** on SBA-15 type silica.

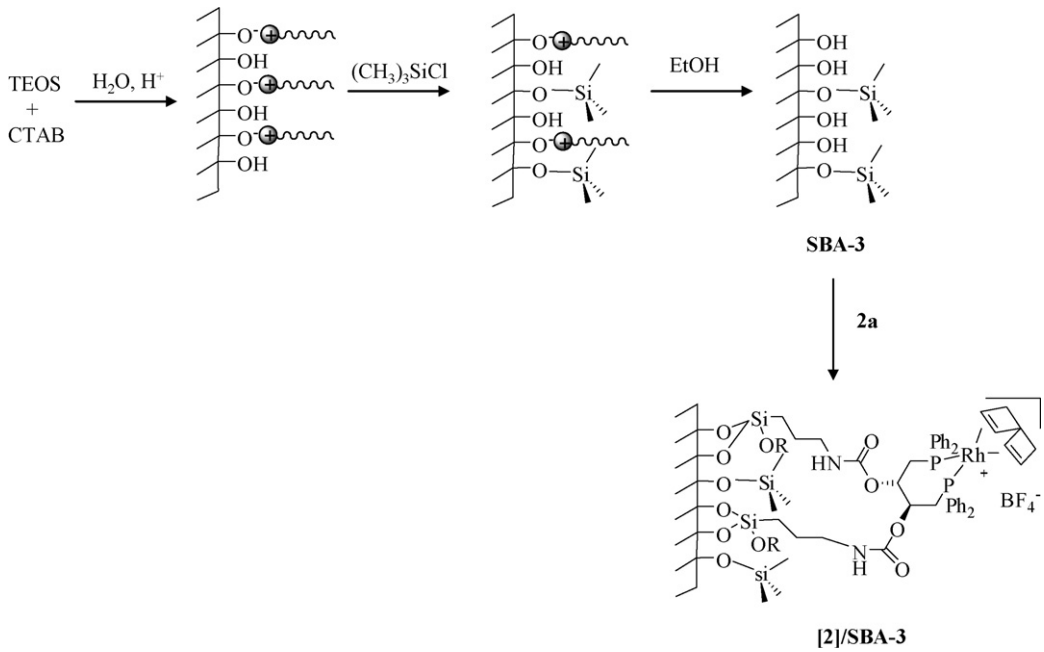

Scheme 3. Grafting of rhodium complex **2** on partially silylated SBA-3 type silica.

tant was retained in the pores thus creating molecular patterning of the surface. The subsequent elimination of the SDA by successive ethanol extraction cycles led to the liberation of free silanols which were readily reacted with **2** yielding catalytic solid **[2]/SBA-3**.

These hybrid materials were characterized by a variety of spectroscopic (^{31}P, ^{13}C and ^{29}Si CP MAS NMR, X-ray diffraction) and quantitative (TGA/DTA, elemental analysis) techniques.

Figs. 1 and 2 show small-angle powder XRD patterns of SBA-15 and SBA-3 materials, respectively, before and after grafting of **2**. The SBA-15 type solids exhibited typical diffractograms in the 2θ-range of 0.6–3° characteristic of hexagonally ordered mesophases with a d_{100} spacing ranging from 96 to 99 Å (Fig. 1, Table 1). However, a significant decrease in intensity of d_{100} reflection was observed for **[2]/SBA-15** which could be attributed to lower local order and/or due to contrast matching between the amorphous silicate framework and the metal complex located inside the channels. The X-ray diffractograms of SBA-3 type materials exhibited a single peak assigned to the d_{100} reflection of hexagonal symmetry (Fig. 2). After the post-synthetic grafting of **2**, a clear shift to higher 2θ values was observed compared to parent SBA-3 (from 34.4 to 32.2 Å for d_{100} reflection, Table 1). These changes could result from a contraction of the pore volume of the grafted sample due to the immobilization of bulky rhodium complex in the channels. Note that this phenomenon is less noticeable in the case of SBA-15 hybrid materials arising probably from the large pore size of these latter.

The textural data derived from the BET analysis of nitrogen adsorption and desorption experiments are presented in Table 1. All the materials exhibited type IV isotherms characteristic of mesoporous solids according to IUPAC classification [24] (Supporting Information, Figs. S3 and S4 for graphical data). Concerning SBA-15 solids, nitrogen adsorption-desorption isotherms displayed sharp steps with hysteresis loops at relative pressure in the range of 0.6–0.8 corresponding to the filling of the ordered pores (Fig. S3, right). Large pore diameters ranging from 62 to 69 Å were

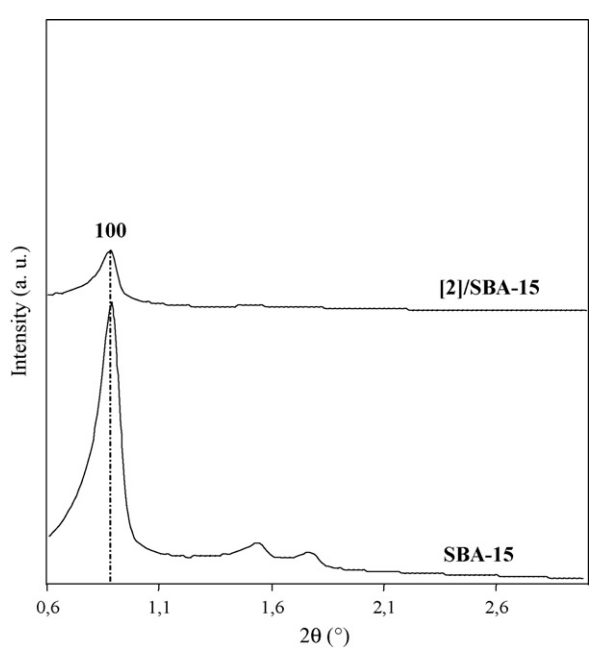

Fig. 1. X-ray powder diffraction pattern of SBA-15 materials before (bottom) and after grafting of **2** (top).

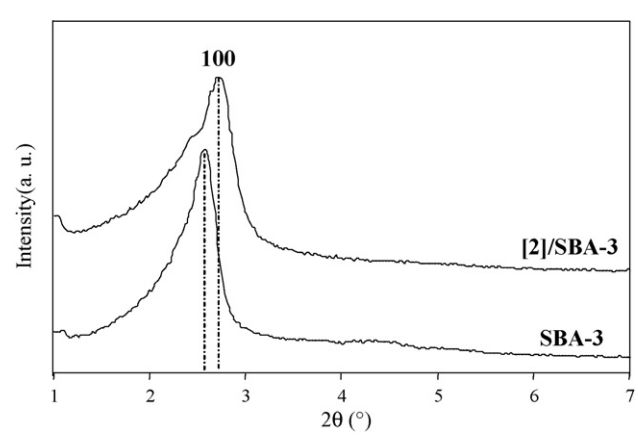

Fig. 2. X-ray powder diffraction pattern of SBA-3 materials before (bottom) and after grafting of **2** (top).

Table 1
Physical and textural properties of chiral rhodium diphosphine complex **2** functionalized SBA-15 and SBA-3 type silica materials.

Sample	wt% Rh	Structural and textural properties							
		d_{100}[a] (Å)	a_0[b] (Å)	Wall thickness[c] (Å)	$V\mu$[d] ($cm^3\,g^{-1}$)	V_p[e] ($cm^3\,g^{-1}$)	D_p[f] (Å)	S_{BET} ($m^2\,g^{-1}$)	C_{BET}
SBA-15		96.2	111.1	48.1	0.08	1.09	63	844	189
[2]/SBA-15	1.5	98.9	114.4	52.2	0.01	0.76	62	508	76
SBA-3		34.4	39.7	17.7	0.4	0.50	22	1014	40
[2]/SBA-3	2.75	32.2	37.2	15.2	0.16	0.20	22	437	34

[a] $d(1\,0\,0)$ spacing.
[b] $a_0 = 2d(1\,0\,0)/\sqrt{3}$, hexagonal lattice parameter calculated from XRD.
[c] Calculated by a_0 − pore size.
[d] Micropore volume determined using the *t*-plot method.
[e] Total pore volume at $P/P_0 = 0.980$.
[f] Pore size from desorption branch applying the BJH pore analysis.

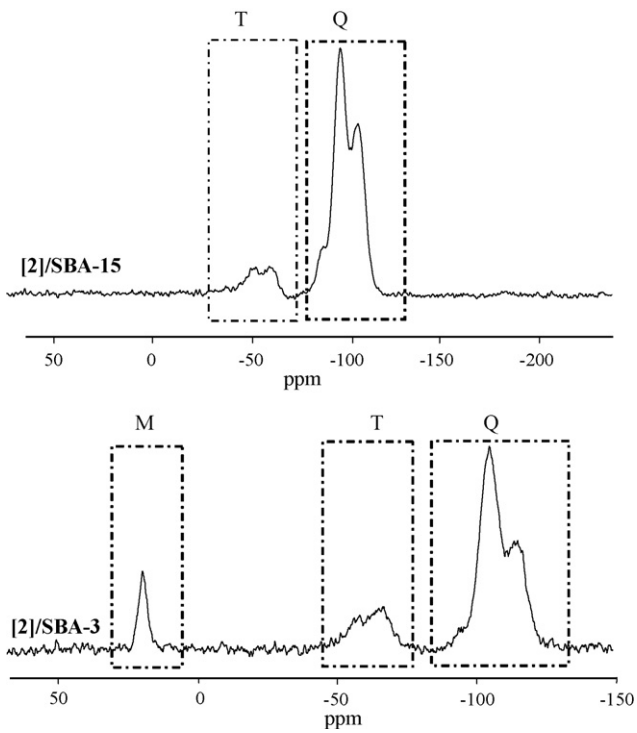

Fig. 3. CP-MAS ^{29}Si NMR of **2** functionalized SBA-15 (top) and SBA-3 (bottom) hybrid materials.

obtained with relatively narrow pore size distribution. The decrease in surface area (e.g. from 844 to 508 $m^2\,g^{-1}$) as well as in pore volume (e.g. from 1.09 to 0.76 $cm^3\,g^{-1}$) observed for **[2]/SBA-15** evidenced that the organometallic complex in grafted solids were mainly located on internal surface of mesoporous materials. In the case of SBA-3 materials, the parent SBA-3 displayed a high BET surface area of 1014 $m^2\,g^{-1}$ with an average pore diameter of 22 Å and a pore volume of 0.5 $cm^3\,g^{-1}$. Upon functionalization with **2**, no change in pore diameter was observed whereas a marked decrease in surface area (437 $m^2\,g^{-1}$) and pore volume (0.2 $cm^3\,g^{-1}$) was obtained consistent with the presence of a significant amount of rhodium on the interior mesopore surfaces. It is also interesting to mention that the wall thickness in the SBA-3 type materials was on average three times smaller than that of the SBA-15 solids.

Confirmation of incorporation of **2** in the pores of the materials was obtained by NMR spectroscopy. Examination of the ^{13}C CP-MAS NMR spectra of the modified solids along with the solution phase spectrum of the corresponding molecular precursor led to the conclusion that the organic fragments in **2** remained intact during the grafting and subsequent workup without measurable decomposition (Supporting Information, Fig. S5). In addition to the peaks attributed to **2** one also discerns the presence of a new resonance at 1 ppm for **[2]/SBA-3** characteristic of the carbons of the trimethylsilyl group of the partially capped silica. Solid-state ^{29}Si NMR provides further information about the silicon environment and the degree of functionalization. In all cases, the organometallic/organic fragment of the precursor molecule was covalently grafted onto the solid, and the precursors were, in general, attached to the surface of the mesoporous oxide by multiple siloxane bridges as evidenced in Fig. 3 by the presence of T^m sites (with $m = 1$–3) in the spectral region ranging from −45 to −70 ppm. Peaks assignable to Q^2, Q^3, and Q^4 silicon sites of the silica framework were also discernible in all four spectra. Additionally, a resonance at 15 ppm assigned to M type silicon and corresponding to grafted trimethylsilyl groups was observed in the ^{29}Si NMR spectrum of **[2]/SBA-3**.

Solid-state ^{31}P NMR spectroscopy proved to be a useful technique to elucidate the structural nature and integrity of the rhodium supported complexes. The ^{31}P MAS NMR spectra of the modified SBA-15 and SBA-3 silica materials are presented together with the liquid ^{31}P NMR spectrum of **2** in Fig. 4. In the case of

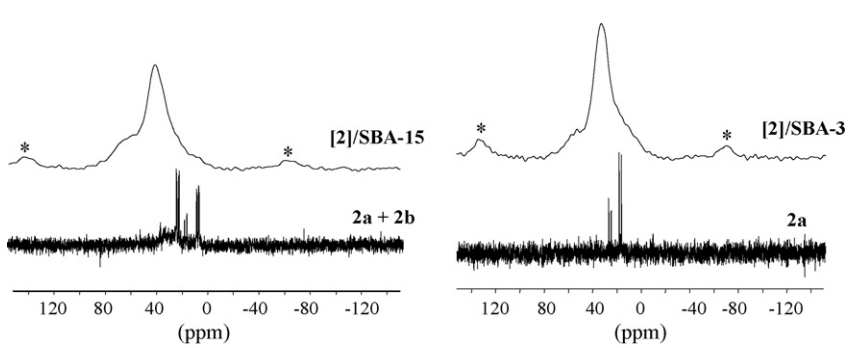

Fig. 4. ^{31}P NMR of molecular rhodium precursor **2** and MAS ^{31}P NMR of **2** modified SBA-15 (left) and SBA-3 (right) type silica materials. *Denotes for spinning side bands.

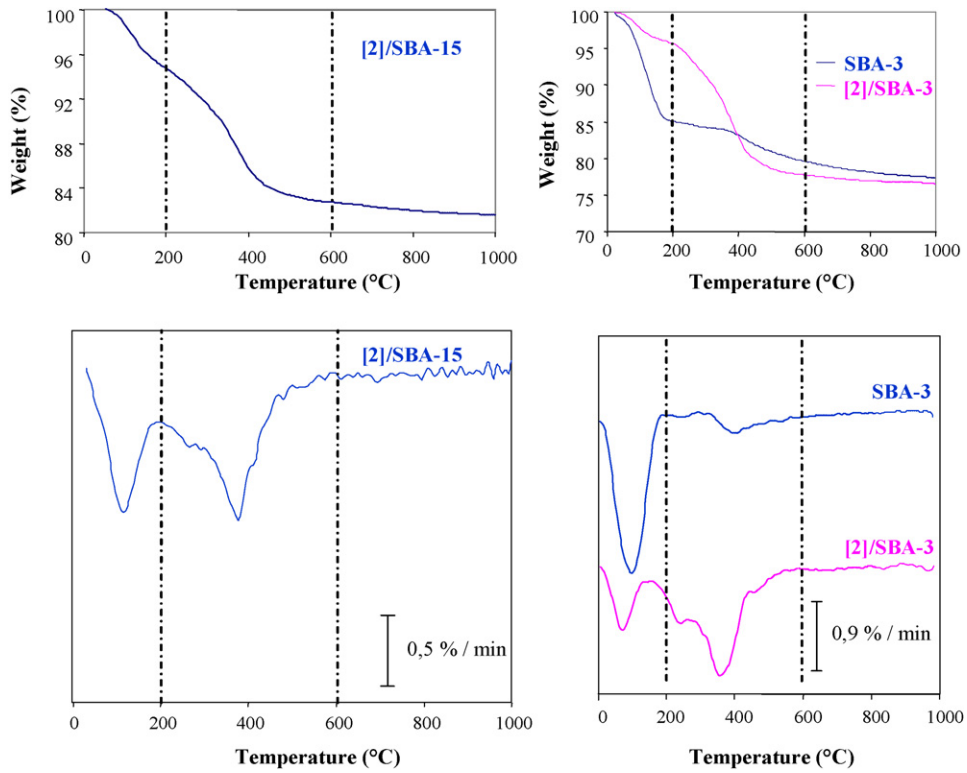

Fig. 5. Representative thermogravimetric weight loss curves (top) and derivatives plots (bottom) for **2** functionalized SBA-15 (left) and SBA-3 (right) silica hybrid materials.

[2]/SBA-3 material (Fig. 4, right) one observes the presence of a relatively broad resonance centered at 32.8 ppm along with a shoulder around 53 ppm and spinning side bands. Unfortunately, the line broadening of the signals, although expected for heterogenized species, prevented an accurate determination of rhodium phosphorus coupling under these conditions. Nevertheless, the Rh–P bond seemed to be not affected during the grafting: free ligand was not detected (δ −23.4) and chemical shifts correspond to coordinated phosphine ligand [25]. The observed broad peaks in the solid state were slightly downfield (17 ppm) from those observed for the molecular species in solution. This may be due to some direct or longer range interaction between the rhodium and the silica surface [12a]. Similar results were obtained for **[2]/SBA-15** material (Fig. 4, left) except that the shift of the ^{31}P signals to lower magnetic field was more pronounced (approximately 31 ppm). This may be ascribed to more intense rhodium–surface oxygen interactions which were less favorable at the partially capped SBA-3 silica surface.

Quantitative determinations of rhodium complex contents for the hybrid materials were performed by thermogravimetric analysis (TG/DTG) in air and elemental analysis. The thermogravimetric data are summarized in Fig. 5 and Table S1 (Supporting Information).

Generally, similar thermal profiles were observed for all the hybrids, composed of three weight loss regions. A first weight loss occurred at temperatures up to about 200 °C and was assigned to the desorption of water. A second weight loss occurred at temperatures ranging from 200 to 600 °C, and this loss presumably arises from the decomposition of the organometallic and organic species and desorption of the volatile decomposition products. Depending on the nature of the organic fragments, several desorption peaks could be observed in this region. In the case of **[2]/SBA-15**, a weight loss of 12 wt% was obtained compared to 19 wt% for **[2]/SBA-3**. Note that the decomposition occurs at elevated temperature (centered at 380 °C) revealing the high thermal stability of the rhodium immobilized materials. The third weight loss region, which took place above 600 °C, was ascribed to the release of water formed from the condensation of silanols in the silica structure. In quantitative terms, one should consider the organic loading of the surface in comparison to the dry mineral weight of the material, in this case, the weight of the material at the end of thermal treatment. Thus, the functional group loading for **[2]/SBA-15** hybrid was found to be 0.15 g/g of dry SiO_2 as determined by TGA (Supporting Information, Table S1). In the case of **SBA-3** derived materials, the rhodium-containing material was derived from an organically capped silica hybrid material precursor. Thus, we can measure the organic content coming from the trimethyl silyl groups prior to the grafting of the rhodium complex and do not depend exclusively on the TGA curve to separate the weight contributions of organic and organometallic fragments in **[2]/SBA-3**. Direct comparison of the weight loss in the 200–650 °C region of **SBA-3** (0.07 g/g SiO_2) and **[2]/SBA-3** (0.24 g/g SiO_2) leads us to the organometallic loading of the material, 0.17 g/g SiO_2.

Elemental analysis of phosphorous, rhodium and boron were obtained for both rhodium-containing materials and are summarized in Table S2 (Supporting Information). **[2]/SBA-15** was found to contain 1.5 wt% Rh with a phosphorus/rhodium molar ratio of 2.1 (expected 2) and a boron/rhodium molar ratio of 1 (expected 1) suggesting that on average one diphosphine ligand and one BF_4^- anion per rhodium atom were left on the surface. The integrity of the molecular precursor **2** was also maintained for **[2]/SBA-3** (P/Rh 1.8; B/Rh 1) with higher rhodium content (2.74 wt% Rh).

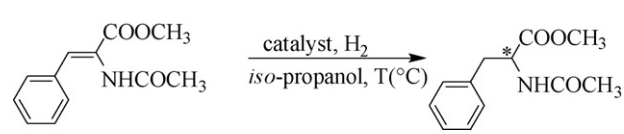

Scheme 4. Rhodium catalyzed hydrogenation of methyl (*Z*)-2-*N*-acetylamino-cinnamate.

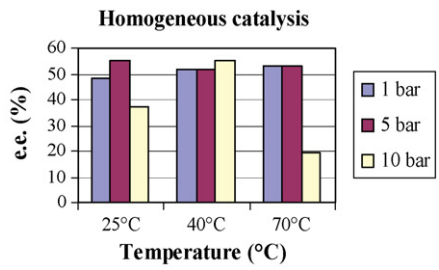

Entry	Pressure H_2 (bar)	Temperature (°C)	e.e. (%)
1	1	25	48 (*R*)
2	1	40	52 (*R*)
3	1	70	53 (*R*)
4	5	25	55 (*R*)
5	5	40	52 (*R*)
6	5	70	53 (*R*)
7	10	25	37 (*R*)
8	10	40	57 (*R*)
9	10	70	19 (*R*)

Fig. 6. Hydrogenation of methyl (*Z*)-2-*N*-acetylaminocinnamate catalyzed by $[Rh(COD)]_2^+BF_4^-$/**1a** system.

Table 2
Hydrogenation of methyl (*Z*)-2-*N*-acetylaminocinnamate catalyzed by **2** functionalized SBA-15 and SBA-3 hybrid materials under various reaction conditions.

Entry	Sample	Pressure H_2 (bar)	Temperature (°C)	Rate[a] (h^{-1})	Time (h)	Conversion [b] (%)	Yield[b] (%)	ee[c] (%)
1	**[2]/SBA-15**	5	25	2.5	120	99	96	4 (*R*)
2	**[2]/SBA-15**	5	40	4.1	40	94	94	5 (*R*)
3	**[2]/SBA-15**	10	40	7.9	24	100	100	3 (*R*)
4	**[2]/SBA-15**	40	40	42.3	24	100	100	3 (*R*)
5	**[2]/SBA-3**	5	25	0.5	48	17	13	20 (*R*)
6	**[2]/SBA-3**	5	40	9.0	48	100	100	6 (*R*)

[a] Initial rates were determined from the kinetic experiments by tracing the tangent at $t = 0$ and account only for the formation of the hydrogenated product.
[b] Conversions based on unreacted methyl (*Z*)-2-*N*-acetamidocinnamate and yields were determined by GC with an internal standard (diethylene glycol di-*n*-butyl ether).
[c] Determined by HPLC using a chiral column.

3.3. Asymmetric hydrogenation

The goal of this work was to examine the influence of the silica support in the Rh-catalyzed hydrogenation of methyl (*Z*)-2-*N*-acetylaminocinnamate using a DIOP derivative as ligand (Scheme 4). This reaction was chosen because it is probably the best known standard hydrogenation reaction, even though it is well known that enantiomeric excesses obtained with this type of ligand are typically modest for this reaction.

In a first series of experiments, we studied homogeneous hydrogenation reactions in isopropyl alcohol catalyzed with 1.0% molar of Rh-catalyst prepared from 1 equiv. of cationic complex $[Rh(COD)_2]^+BF_4^-$ and 1 equiv. of molecular bis-silylated DIOP precursor **1a**. The catalysis was performed under different reaction conditions with varying hydrogen pressure (1, 5 and 10 bar) and temperature (25, 40 and 70 °C) and the results are shown in Fig. 6. As expected, the reaction rate was high and full conversion with quantitative yield in *N*-acetylphenylalanine was obtained after 20 min. The enantiomeric excesses ranging between 48 and 53% in favor of the *R*-enantiomer were not significantly modified when working under 1 or 5 bar of hydrogen. However, under 10 bar of hydrogen, the enantiomeric excesses were strongly dependant on the temperature with a sharp decrease at elevated temperature (19% ee at 70 °C vs. 57% ee at 40 °C). These results are very similar to those already described from DIOP-based ligand [18]. It should also be noted that the enantioselectivity exhibited by DIOP-based catalysts has been shown to be sensitive to slight changes in bite angle [26] and thus slight variation of ee can be considered normal.

Before testing the reactivity of the hybrid catalysts **[2]/SBA-15** and **[2]/SBA-3**, a blank run was performed on the silica support previously dried at 200 °C under nitrogen overnight. Under standard conditions (40 °C, 10 bar H_2) no *N*-acetylphenylalanine product was observed after 24 h of reaction indicating that the silica matrix exhibits no measurable activity toward hydrogenation. We also verified that under the same conditions the cationic complex $[Rh(COD)_2]^+BF_4^-$ did not lead to any enantioselectivity although an average conversion of 54% was obtained. The catalytic results of the Rh-materials **[2]/SBA-15** and **[2]/SBA-3** are depicted in Table 2.

In the case of **[2]/SBA-15** catalyst, full conversion was obtained whatever the experimental conditions used (pressure and temperature) (Table 2, entries 1–4) with 100% selectivity in hydrogenated product (Supporting Information, Fig. S6). However, a very low ee (4–5%) compared to homogeneous system (average 50%) was observed in each case. This decrease in activity and selectivity is frequently observed for heterogenized complexes.

The rate of hydrogenation was strongly dependant on the experimental conditions. A conversion of 99% was determined after 120 h at 5 bar and 25 °C, while total conversion was determined after only 24 h when the pressure of hydrogen and the temperature were raised from 5 to 40 bar and from 25 to 40 °C, respectively (Table 2, entries 1 and 4). As illustrated in Fig. 7 and Table 2, the initial activity followed a similar trend and increased with the temperature of the reaction and the pressure of hydrogen while the ee remained unchanged. Under 5 bar of H_2 and at 25 °C, an initial rate of 2.5 h^{-1} was obtained (Table 2, entry 1), it was improved by a factor of 2

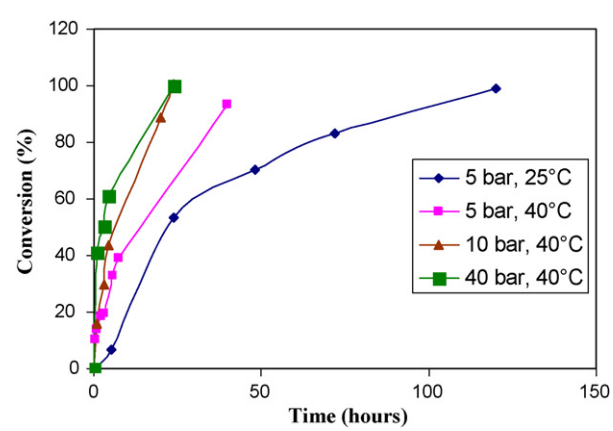

Fig. 7. Hydrogenation of methyl (*Z*)-2-*N*-acetylaminocinnamate catalyzed by **[2]/SBA-15** hybrid material at various pressure and temperature.

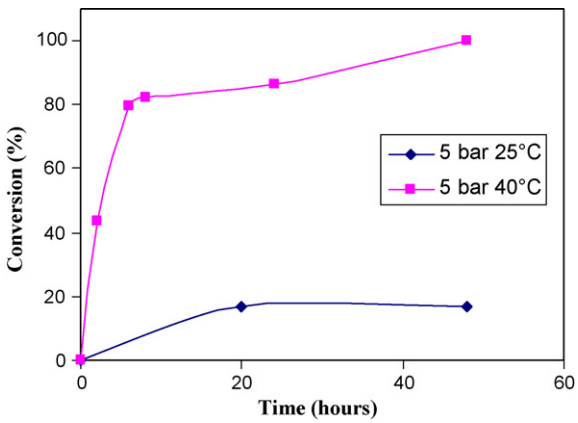

Fig. 8. Hydrogenation of methyl (*Z*)-2-*N*-acetylaminocinnamate catalyzed by **[2]/SBA-3** hybrid material.

when the temperature was increased to 40 °C (Table 2, entry 2) and by a factor of 3 by further increasing the hydrogen pressure to 10 bar (Table 2, entry 3), the best results being obtained under 40 bar of H_2 and at 40 °C with an initial rate of 42.3 h^{-1} (Table 2, entry 4).

For comparison, hybrid material **[2]/SBA-3** was submitted to the same standard conditions. A low conversion of 17% was obtained when the reaction was performed at 5 bar of hydrogen and at 25 °C with an initial rate of 0.5 h^{-1} (Table 2, entry 5). This relatively low activity could stem from a restricted accessibility to the catalytic sites. Recall that the silica surface in **[2]/SBA-3** is somewhat hydrophobic which could make more difficult the transport and adsorption of polar substrate within the catalytic material. Under these conditions however enantioselectivity up to 20% was achieved which represents the best ee obtained in this series of heterogeneous catalysts (Table 2, entry 5). The higher confined space in **[2]/SBA-3** (pore diameter of 22 Å) compared to **[2]/SBA-15** (pore diameter of 62 Å) may lead to a larger influence of the chiral directing group on the orientation of the substrate relative to the metal center. To achieve full conversion, it was necessary to increase the temperature to 40 °C (Table 2, entry 6 and Fig. 8). Unfortunately, the increase in the reaction rate (9.0 h^{-1} vs. 0.5 h^{-1}) was made at the expense of the enantioselectivity which dropped to 6%.

4. Conclusion

Heterogeneous chiral cationic rhodium complexes bearing bidentate phosphine derived from DIOP were prepared by covalent immobilization onto SBA type silica. The DIOP ligand was modified in two steps to introduce polycondensable organosiloxane precursor moieties. Subsequent complexation with $Rh(COD)_2{}^+BF_4{}^-$ afforded the targeted rhodium complex which was then grafted onto two types of silica materials which varied in terms of pore diameter and surface hydrophilicity. These hybrids were tested as catalysts for the enantioselective hydrogenation of methyl (*Z*)-2-*N*-acetylaminocinnamate, a benchmark reaction for C=C reduction. The material having no surface passivation produced very little enantioselectivity compared to the homogeneous analog. Surface passivation ameliorated the performance of the catalyst, but the enantioselectivity remains disappointing. Current studies concentrate on an approach to heterogenization by incorporating the covalent link to the surface by a monodentate phosphine ligand rather than through the chiral auxillary DIOP.

Acknowledgement

RS thanks the French Ministry of Superior Education and Research for a fellowship.

Appendix A. Supplementary data

Supplementary data associated with this article can be found, in the online version, at doi:10.1016/j.molcata.2009.08.025.

References

[1] (a) N.E. Leadbeater, M. Marco, Chem. Rev. 102 (2002) 3217–3273;
(b) Q.H. Fan, Y.M. Li, A.S.C. Chan, Chem. Rev. 102 (2002) 3385–3466;
(c) C.E. Song, S.G. Lee, Chem. Rev. 102 (2002) 3495–3524;
(d) Z.-I. Lu, E. Lindler, H.A. Mayer, Chem. Rev. 102 (2002) 3543–3578;
(e) A.P. Wight, M.E. Davis, Chem. Rev. 102 (2002) 3589–3614;
(f) D.E. De Vos, M. Dams, B.F. Sels, P.A. Jacobs, Chem. Rev. 102 (2002) 3615–3640.
[2] (a) R. Haag, S. Roller, Top. Curr. Chem. 242 (2004) 1–42;
(b) Y. Uozumi, Top. Curr. Chem. 242 (2004) 77–112;
(c) D.E. Bergbreiter, Top. Curr. Chem. 242 (2004) 113–176;
(d) N. End, K.-U. Schöning, Top. Curr. Chem. 242 (2004) 242–271.
[3] D.J. Gravert, K.D. Janda, Chem. Rev. 97 (1997) 489–510.
[4] P. McMorn, G.J. Hutchings, Chem. Soc. Rev. 33 (2004) 108–122.
[5] H.B. Kagan, T.-P. Dang, J. Am. Chem. Soc. 94 (1972) 6429–6433.
[6] (a) W.S. Knowles, M.J. Sabacky, B.D. Nineyard, J. Chem. Soc., Chem. Commun. (1972) 10–11;
(b) B.D. Vineyard, W.S. Knowles, M.J. Sabacky, G.L. Bachman, D.J. Weinkauff, J. Am. Chem. Soc. 99 (1977) 5946–5952.
[7] M.D. Fryzuk, B. Bosnich, J. Am. Chem. Soc. 99 (1977) 6262–6267.
[8] (a) M.J. Burk, J.E. Feaster, R.L. Harlow, Organometallics 9 (1990) 2653–2655;
(b) M.J. Burk, J. Am. Chem. Soc. 113 (1991) 8518–8519;
(c) M.J. Burk, J.E. Feaster, W.A. Nugent, R.L. Harlow, J. Am. Chem. Soc. 115 (1993) 10125–10138;
(d) M.J. Burk, J.R. Lee, J.P. Martine, J. Am. Chem. Soc. 116 (1994) 10847–10848;
(e) M.J. Burk, Y.M. Wang, J.R. Lee, J. Am. Chem. Soc. 119 (1996) 5142–5143.
[9] (a) A. Miyashita, A. Yasuda, H. Takaya, K. Toriumi, T. Ito, T. Souchi, R. Noyori, J. Am. Chem. Soc. 102 (1980) 7932–7934;
(b) A. Miyashita, H. Takaya, T. Souchi, R. Noyori, Tetrahedron 40 (1984) 1245–1253;
(c) H. Takaya, K. Mashima, K. Koyano, M. Yagi, H. Kumobayashi, T. Takemomi, S. Akutagawa, R. Noyori, J. Org. Chem. 51 (1986) 629–635.
[10] R. Augustine, S. Tanielyan, S. Anderson, H. Yang, Chem. Commun. (1999) 1257–1258.
[11] F.M. de Rege, D.K. Morita, K.C. Ott, W. Tumas, R.D. Broene, Chem. Commun. (2000) 1797–1798.
[12] (a) H.H. Wagner, H. Hausmann, W.F. Hölderich, J. Catal. 203 (2001) 150–156;
(b) W.P. Hems, P. McMorn, S. Riddel, S. Watson, F.E. Hancock, G.J. Hutchings, Org. Biomol. Chem. 3 (2005) 1547–1550.
[13] C. Simons, U. Hanefeld, I.W.C.E. Arends, R.A. Sheldon, T. Maschmeyer, Chem. Eur. J. 10 (2004) 5829–5835.
[14] S.A. Raynor, J.M. Thomas, R. Raja, B.F.G. Johnson, R.G. Bell, M.D. Mantle, Chem. Commun. (2000) 1925–1926.
[15] C.M. Crudden, D. Allen, M.D. Mikoluk, J. Sun, Chem. Commun. (2001) 1154–1155.
[16] J.P. Collman, J.A. Belmont, J.I. Brauman, J. Am. Chem. Soc. 105 (1983) 7288–7294.
[17] I. Steiner, R. Aufdenblatten, A. Togni, H.-U. Blaser, B. Pugin, Tetrahedron: Asymmetry 15 (2004) 2307–2311.
[18] (a) W. Hu, C.-C. Chen, G. Xue, A.S.C. Chan, Tetrahedron: Asymmetry 9 (1998) 4183–4192;
(b) F. Robert, G. Oehme, D. Sinou, J. Mol. Catal. A: Chem. 139 (1999) 105–108;
(c) W. Li, X. Zhang, J. Org. Chem. 65 (2000) 5871–5874.
[19] A.M.d'A. Rocha Gonsalves, J.C. Bayón, M.M. Pereira, M.E.S. Serra, J.P.R. Pereira, J. Organomet. Chem. 553 (1998) 199–204.
[20] (a) R.R. Schrock, J.A. Osborn, J. Am. Chem. Soc. 93 (1971) 2397–2407;
(b) D. Moulin, C. Darcel, S. Jugé, Tetrahedron: Asymmetry 10 (1999) 4729–4743.
[21] A. Kawazaki, K. Maekawa, K. Kubo, T. Igarashi, T. Sakurai, Tetrahedron 60 (2004) 9517–9524.
[22] (a) D. Zhao, J. Feng, Q. Huo, N. Melosh, G.H. Fredrickson, B.F. Chmelka, G.D. Stucky, Science 279 (1998) 548–552;
(b) D. Zhao, Q. Huo, J. Feng, B.F. Chmelka, G.D. Stucky, J. Am. Chem. Soc. 120 (1998) 6024–6036;
(c) D. Zhao, J. Sun, Q. Li, G.D. Stucky, Chem. Mater. 12 (2000) 275–279.
[23] (a) V. Dufaud, F. Beauchesne, L. Bonneviot, Angew. Chem. Int. Ed. Engl. 44 (2005) 3475–3477;
(b) V. Dufaud Niccolai, L. Bonneviot, Preparation of multi-functionalized porous silica mesostructures using polycondensation in micellar surfactant and functionalizations Fr. Demande, 2006, FR 2878518, 58 pp.
[24] S.J. Gregg, K.W. Sing, Adsorption Surface Area and Porosity, second ed., Academic Press, London, 1982.
[25] D.A. Slack, I. Greveling, M.E. Baird, Inorg. Chem. 18 (1979) 3125–3132.
[26] (a) P. Dierkes, P.W.N.M. van Leeuwen, J. Chem. Soc., Dalton Trans. (1999) 1519–1529;
(b) Z. Freixa, P.W.N.M. van Leeuwen, Dalton Trans. 1890 (2003) 1901.